Contact position analysis of deep brain stimulation electrodes on post-operative CT images

Simone Hemm, Jérôme Coste, Jean Gabrillargues, Lemlih Ouchchane, Laurent Sarry, François Caire, François Vassal, Christophe Nuti, Philippe Derost, Franck Durif, et al.

Contact position analysis of deep brain stimulation electrodes on post-operative CT images

Simone Hemm (1,2), Jérôme Coste (1,2), Jean Gabrillargues (1,3), Lemlih Ouchchane (1,4), Laurent Sarry (1), François Caire (1,5), François Vassal (1,6), Christophe Nuti (1,6), Philippe Derost (7), Franck Durif (7), Jean-Jacques Lemaire (1,2,*)

1.Inserm, ERI 14, Equipe de Recherche en Imagerie Médicale, Clermont-Ferrand, France

2.CHU Clermont-Ferrand, Hôpital Gabriel-Montpied, Service de Neurochirurgie A, Clermont-Ferrand, France

3.CHU Clermont-Ferrand, Hôpital Gabriel-Montpied, Service de Radiologie A, Clermont-Ferrand, France

4.Université Clermont-Ferrand 1, UFR Médecine, Unité de Bio statistiques, télématique et traitement d'image, Clermont-Ferrand, France

5.CHU Limoges, Hôpital Dupuytren, Service de Neurochirurgie, Limoges, France

6.CHU Saint-Etienne, Hôpital Hôpital Bellevue, Service de Neurochirurgie, Saint-Etienne, France

7.CHU Clermont-Ferrand, Hôpital Gabriel-Montpied, Service de Neurologie, Clermont-Ferrand, France

* jjlemaire@chu-clermontferrand.fr

KEYWORDS: Electrode artefact, STN-DBS, CT, Position analysis

ABSTRACT

Purpose

Groups performing deep brain stimulation advocate post-operative imaging [magnetic resonance imaging (MRI) or computer tomography (CT)] to analyse the position of each electrode contact. The artefact of the Activa 3389 electrode had been described for MRI but not for CT. We undertook an electrode artefact analysis for CT imaging to obtain information on the artefact dimensions and related electrode contact positions.

Methods

The electrode was fixed on a phantom in a set position and six acquisitions were run (in-vitro study). The artefacts were compared with the real electrode position. Ten post-operative acquisitions were analysed (in-vivo analysis). We measured: *H* (height of the lateral black artefact), *D* (distance between the beginning of the white and the lateral black artefacts) and *W* (maximal artefact width), representing respectively the lengths of the four contacts and the electrode tip and width of the contact zone. A Student *t*-test compared the results: in vivo vs in vitro and coronal vs sagittal reconstructions along the electrode.

Results

The limits of the lateral black artefact around the electrode contacts corresponded to the final electrode position. There was no significant difference for *D* (in vivo, 1.1 ± 0.1 mm; in vitro, 1.2 ± 0.2 mm; $p = 0.213$), while *W* and *H* differed slightly (in vivo, $W = 3.3 \pm 0.2$ mm, $H = 7.7 \pm 0.2$ mm; in vitro, $W = 3.1 \pm 0.1$ mm, $H = 7.5 \pm 0.2$ mm). Results obtained with sagittal and coronal reconstructions were similar ($p > 0.6$).

Conclusions

Precise three-dimensional (3D) localisation of the four-contact zone of the electrode can be obtained by CT identification of the limits of the lateral black artefact. The relative position of the four contacts is deduced from the size of the contacts and the inter-contact distance. Sagittal and coronal reconstructions along the electrode direction should be considered for the identification of the four electrode contacts. CT offers a useful alternative to post-operative MRI.

INTRODUCTION

Deep brain stimulation (DBS) of various brain structures is widely used to treat movement disorders [4, 6, 10, 20]. However, the precise anatomical structures with their related functional circuitry affected by stimulation, and so the underlying mechanisms of action of DBS, have not yet been identified [1, 2]. The success of DBS electrode implantation is essentially appraised by the relief of symptoms, but the position of electrode contacts needs to be determined in terms of anatomical position. More and more groups advocate post-operative imaging [magnetic resonance imaging (MRI) or computer tomography (CT)] to check for the absence of haemorrhage, determine the final electrode position compared with the planned one and perform a detailed analysis of the anatomical position of each contact [3, 5, 7, 12, 14, 19]. On post-operative MRI and CT images, the electrode induces an artefact that exceeds the real electrode size to a varying degree. To avoid imprecise three-dimensional (3D) localisation, the electrode position in relation to these artefacts has to be known exactly. Pollo et al. [15] analysed the real electrode position within the MRI artefact in an in-vivo and an in-vitro study. However, serious adverse effects related to MRI acquisition with implanted neurostimulation devices are reported [16], prompting recommendations by the supplier (http://www.medtronic.com/physician/activa/downloadablefiles/196813_a_004.pdf) and specified by governmental organizations (e.g. the French health products safety agency). They focus on the risk of electrode heating during MRI acquisitions and recommend lower specific absorption rates (SARs) for the head than previously accepted (SAR $\leq$ 0.1 W/kg instead of $\leq$ 0.4 W/kg). Given these restrictions, post-operative CT imaging could be a good alternative in practice. Accordingly, we undertook an in-vitro and in-vivo study based on CT images to provide information on the artefact dimensions and related electrode contact positions.

MATERIALS AND METHODS

Electrode

The implanted Activa 3389 electrode (Medtronic, Minneapolis, Minn., USA) is composed of four ring-shaped stimulating contacts [distal (contact 0) to proximal (contact 3)] made of a platinum/iridium alloy. Each contact is 1.5 mm high and 1.27 mm wide. The distance from the distal end of contact 0 to the proximal end of contact 3 is 7.5 mm. Two adjacent contacts are

placed 0.5 mm apart. The two ends of the electrode are interconnected by thin platinum/iridium alloy wire. The electrode tip diameter (beyond the distal contact) is 1 mm.

In-vitro CT study

The localizer

The CT acquisition was run using a phantom (Brainlab, Munich, Germany) containing an in-house support with calibrated holes. The quadripolar electrode was fixed in the middle between two series of holes, with the distal limit of contact 0 just on the line connecting the centres of two holes (Fig. 1).

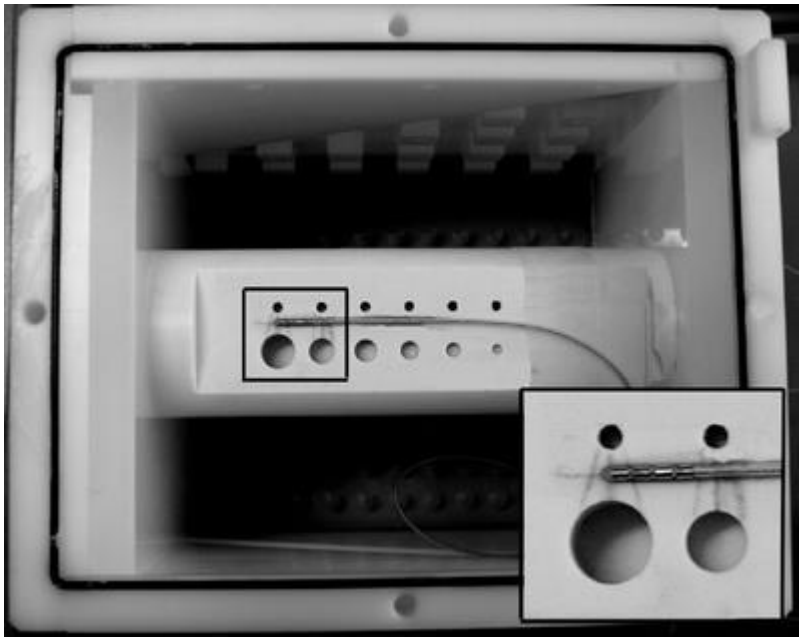

Figure 1. Adapted BrainLab (Munich, Germany) imaging phantom. The distal limit of contact 0 is fixed at the level of the centres of two calibrated holes.

CT acquisition

CT images (Lightspeed, GE) were obtained using the following scan variables: rotation time 1 s, tube voltage 140 kV, effective current 280 mA, Dfov (detailed field of view) 22 cm (containing the whole phantom), matrix 512^2, slice thickness 1.25 mm and slice every 0.6 mm. Images were reconstructed with an isotropic voxel of 0.43 mm^3. Six non-consecutive acquisitions were run using these parameters.

Analysis

First, we identified the plane passing through the middle of the artefact (saturated image), which could serve to represent the electrode centre (iPlan, Brainlab, Feldkirchen, Germany). Images were reoriented along the electrode axis. We identified the plane perpendicular to it just below the line through the centre of the two holes of the support and indicating the distal end of contact 0. A side-by-side visualisation of the photo taken of the experimental set-up and the CT acquisition in the same plane was used for assistance (Fig. 2). The other contacts could then be deduced.

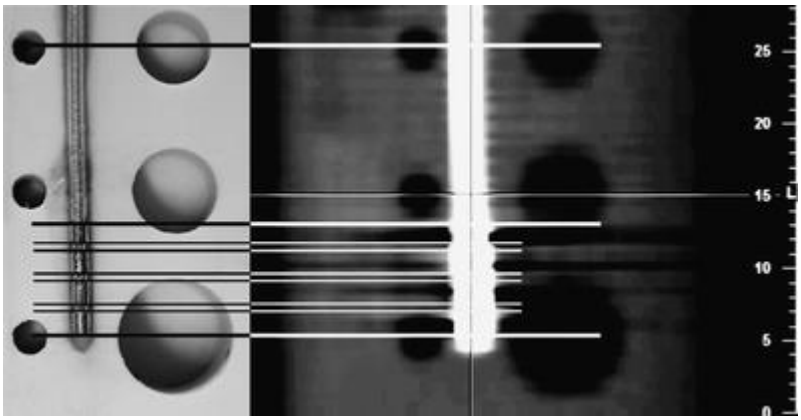

Figure 2. Electrode position analysis within the artefact. Left: Photo of the experimental set-up with the fixed electrode between the calibrated holes. Right: Electrode artefact and calibrated holes on the CT images. The upper and lower bold lines of the contact area represent the distal limit of contact 0 and the proximal limit of contact 3 respectively. The thin lines indicate the other contact ends based on the identification on the photo.

We analysed the real contact position in relation with the lateral black artefact. We measured its height *H* along the electrode axis (Fig. 3). We determined the maximal width of the white electrode artefact (*W*) orthogonal to the main axis of the electrode on pseudo-sagittal and pseudo-coronal reconstructions (saturated image) along the electrode axis. As a third variable, we measured the distance *D* between the beginning of the white electrode artefact and the beginning of the lateral black artefact (Fig. 3), i.e. the electrode tip beyond the distal contact artefact.

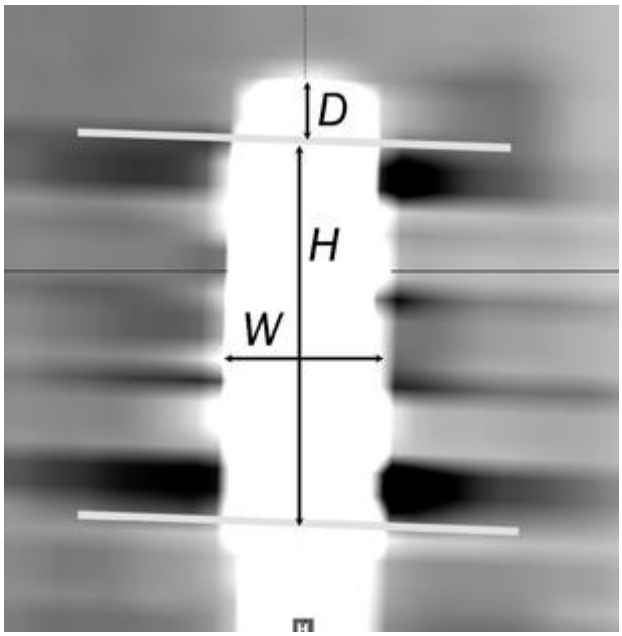

Figure 3. Illustration of the different artefact parameters measured on phantom and patient CT acquisitions. W maximal width of the white electrode artefact, H height of lateral black artefact along the electrode axis, D distance between the beginning of the white electrode artefact and the beginning of the lateral black artefact.

In-vivo CT study

The same CT sequence as described above was run post-operatively in ten patients suffering from idiopathic Parkinson's disease and treated by bilateral subthalamic nucleus (STN) high-frequency stimulation. We determined the plane along the main axis of the electrode. Sagittal and coronal views were reoriented along the main axis for analysis. We measured *H*, *W* and *D* as in the phantom studies in the coronal and sagittal reoriented slices. We visually analysed the influence of the lateral artefact of the second electrode on the artefact of the first one.

Statistical analysis

A Student *t*-test was used to compare *H*, *W* and *D* measured on pseudo-coronal and sagittal reconstructions. A Student *t*-test was also applied to compare in-vitro and in-vivo values of *H*, *W* and *D*.

RESULTS

In-vitro study

From the known electrode position in the phantom study in relation to the artefacts, we sought representative characteristics to allow the identification of the electrode position based on the artefacts alone.

The side-by-side analysis of the photo and the CT acquisition of the phantom showed that the beginning and end of the lateral black artefact corresponded to the ends of the electrode. The protuberances of the white electrode artefact seem to be due to the transition from insulation to contact and vice versa. However, it is not possible to deduce the position of each contact from the horizontal artefact lines as there was no exact correspondence with the known position of the electrode contacts (Figs. 2, 4), except for the proximal and distal black artefact boundaries [respectively, the beginning of the proximal contact (3) and the end of the distal contact (0)]. The mean values of *W*, *H* and *D* for the six acquisitions were 3.1 ± 0.1, 7.5 ± 0.2 and 1.1 ± 0.1 mm (mean ± SD), respectively.

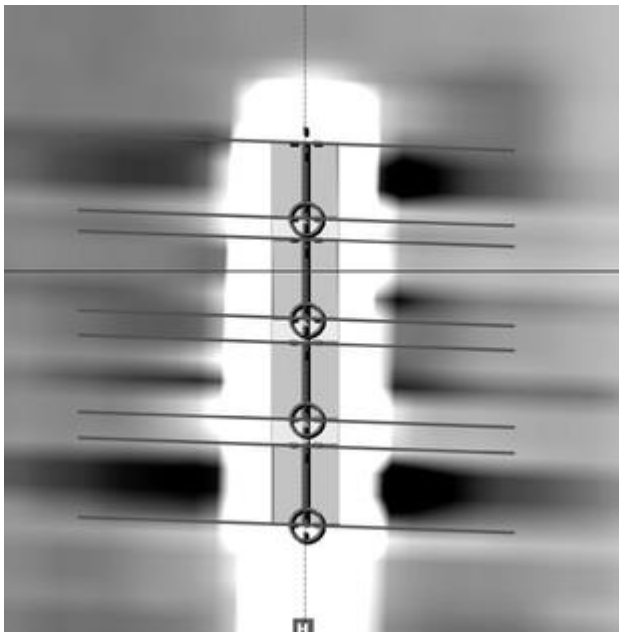

Figure 4. Projection of the four contacts on the electrode CT artefact: the location of the distal and proximal contacts (0 and 3) was deduced from the lateral black artefacts. The representation of the four contacts (grey) was displayed on the same scale as the CT image.

In-vivo study

The visual analysis of the lateral black artefact revealed a difference in orientation compared with that of the phantom study. In the phantom the artefact was nearly perpendicular to the electrode axis, but was tilted in the patient acquisitions (Fig. 5).

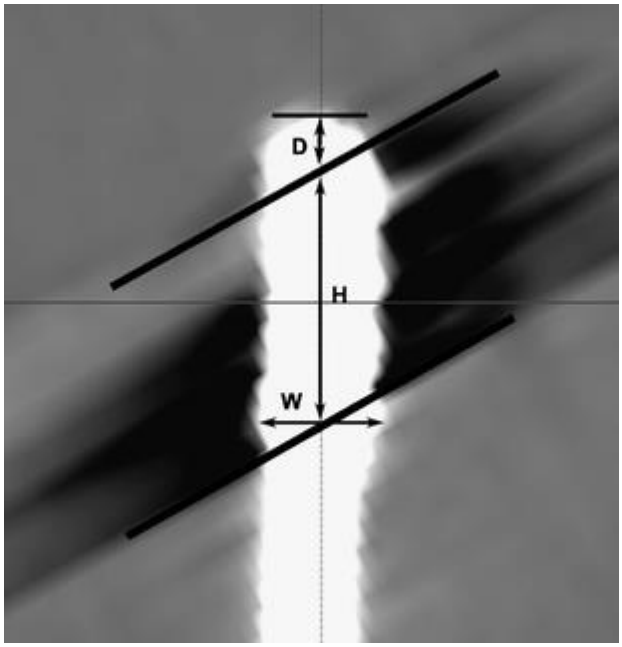

Figure 5. Patient acquisition: tilted lateral black artefact.

Mean values and standard deviation of *W*, *H* and *D* in the sagittal and coronal reconstruction for the 20 electrodes were 3.3 ± 0.2, 7.7 ± 0.2 and 1.2 ± 0.2 mm respectively. The values from in-vivo and in-vitro measurements obtained for *D* showed no significant difference ($p = 0.213$). *W* and *H* differed slightly between in-vivo and in-vitro acquisitions ($p < 0.05$), with respective values of: $W = 3.3 \pm 0.2$ mm, $H = 7.7 \pm 0.2$ mm and $W = 3.1 \pm 0.1$ mm, $H = 7.5 \pm 0.2$ mm. The statistical analysis showed no significant difference in *W*, *D* and *H* between the sagittal and the coronal reconstruction along the electrode direction in the in-vivo and the in-vitro study, with respective *p* values of 0.671, 0.934 and 0.827.

The visual analysis of the mutual influence of the two electrode artefacts showed that the lateral black artefacts of both crossed the whole image, although the artefact decreased in intensity with increasing distance from the electrode (Fig. 6). In the pseudo-coronal direction, a slight superimposition of the two artefacts could thus occur.

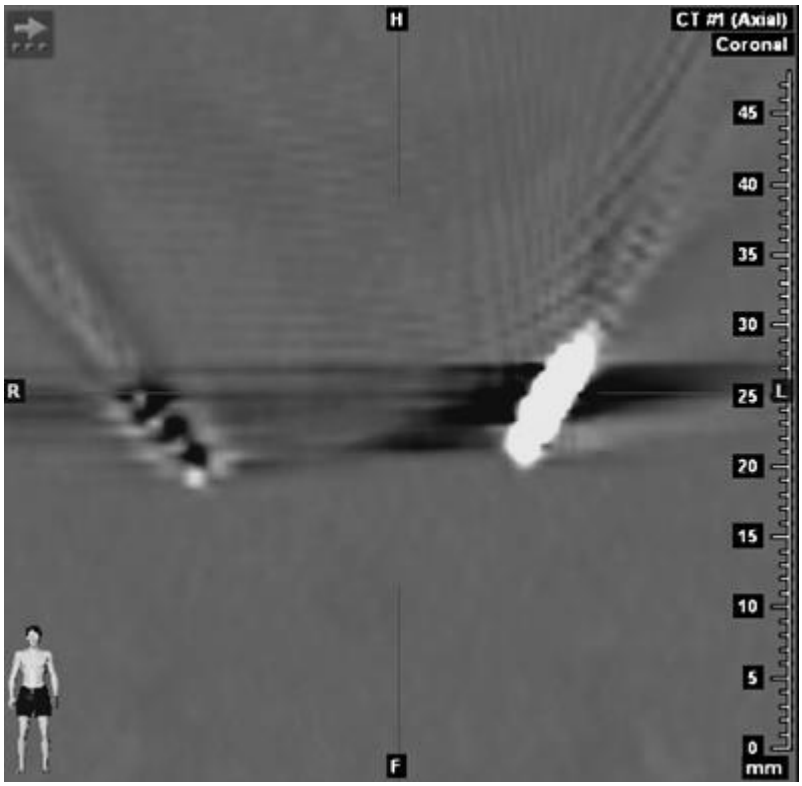

Figure 6. Electrode artefacts after bilateral electrode implantation. The lateral black artefact of one electrode is slightly superimposed on that of the second electrode.

DISCUSSION

Implantation of deep brain stimulation electrodes based on pre-operative MRI has been shown to be efficient in the treatment of movement disorders. Today, nearly all groups include MRI in their targeting concept, as it provides detailed information on the anatomical structures liable to be involved in stimulation. The percentage of groups using additional post-placement imaging is increasing. More and more of these groups are becoming aware of the need for a detailed analysis of the anatomical position of the different electrode contacts to obtain a fuller understanding of deep brain stimulation. They mostly use post-operative MRI [3, 12, 13, 19] or X-ray monitoring [9, 21], but CT acquisitions only rarely [11]. On the 2D X-ray images where electrode contacts are visible separately, stereotactic coordinates of each contact can in general be identified and projected onto the pre-operative image dataset. How to identify the electrode contacts on post-operative MR images has been described by Pollo et al. [15]. As no information is available in the literature on the electrode artefact on CT images, and as CT images are a useful alternative to MR imaging, we set out to analyse the position of the electrode contacts in the artefact.

Phantom and patient CT acquisitions showed the presence of a white artefact corresponding to the electrode and a lateral black artefact around a part of the electrode due to the large difference in density between the contacts and the surrounding tissue. Pollo et al. [15] report that on MRI acquisitions the overlapping of ellipsoid-shaped artefacts of the different contacts gives rise to a larger artefact directly around the contact rather than at the insulation level. On CT images, the zones of protuberances of the white electrode artefact do not correspond to the contacts. They are caused by the transition from metal to insulation. The orientation of the black artefact, and thus the form of the white one, depends on the CT acquisition direction. A tilted orientation with respect to the electrode axis makes the artefact analysis, i.e. determining the end of the black artefact, more difficult, and the white artefact seems larger. This could explain the slight difference in H and W of the artefact between the in-vivo and in-vitro studies. Phantom CT acquisitions confirm that the lateral artefact height H is representative for the position of the four contacts. Although the in-vivo mean value lies slightly above the theoretical 7.5 mm, it remains an acceptable limit of precision, taking into account the limits of resolution and X-ray diffusion. Also, the manufacturing precision of the electrodes seems to be limited and differences in the distances between the contacts are often observed visually during surgery; we used the same

electrode for the six phantom studies, while the in-vivo study used 20 different ones. The width of the artefact is nearly twice the theoretical electrode diameter. This is probably due to X-ray diffusion, the effect of which is stronger in the acquisition direction than in the perpendicular one. While *H* and *W* differ slightly between the in-vivo and the in-vitro study, no significant difference was observed for the electrode tip *D*. Consequently, contact positions analysis relied on (Fig. 7): (1) the identification of the end of the distal contact (contact 0) corresponding to the distal boundary of the lateral black artefact; the tip length of approximately 1.2 mm can be used to validate the beginning of this black artefact; (2) the identification of the beginning of the proximal contact (3; connected to the wire, also producing an artefact, albeit smaller) corresponding to the proximal boundary of the lateral black artefact; (3) the calculation of the four contact locations according to the specified electrode geometry. As there might obviously be a discrepancy between the extremities of the distal and proximal contacts and their respective black artefact boundaries (the lower artefact tilt, the better correspondence between contacts and artefact) we recommend using the point M (the midpoint between the distal and proximal black artefact boundaries) as a reference to calculate the location of the four contacts.

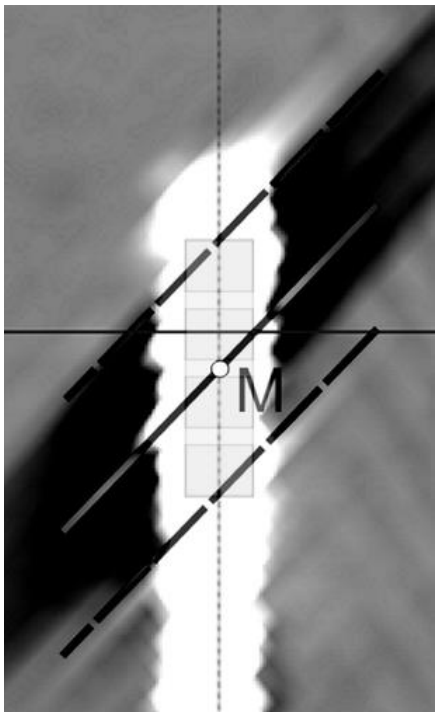

Figure 7. After identification of the distal and proximal black artefact boundaries (dotted lines), the location of the four contacts is determined relatively to the point (M) placed in the middle of the distance between the two boundaries.

As there was no significant difference in mean values between the pseudo-sagittal and the pseudo-coronal directions along the electrode, both can and should be used for the initial contact tip detection. The slight influence of the second electrode in the pseudo-coronal direction should be kept in mind.

CT can offer a useful alternative to post-operative MRI. The advantage of CT over MRI is first of all the acquisition time (<1 min vs <5 min). Also, CT availability is greater than MR accessibility in general and costs less. For the anatomical position analysis, it makes no difference whether postoperative MR or CT images are used, as even with post-operative MR images an image fusion with the pre-operative MRI is necessary to visualise the region of interest without the electrode artefact. Ideally, anatomical position analysis should be performed directly on postoperative images containing both electrode artefacts and anatomical information. However currently, the SAR constraints (≤0.1 W/kg) limit this option with MRI (the electrode artefact remains still too large compared with the structure size) and CT does not allow to see the anatomy; as a consequence, matching post/pre-implantation imaging seems still the simplest way to locate a given contact. Concerning the mutual information algorithm [22] often applied for this kind of image fusion, the precision should be similar for non-distorted CT and MR images, as the algorithm takes into account only the information contained in the images and not the image modality. In addition, the height of the electrode artefact to be considered on CT images is smaller than that on MR images ($H_{MRI} = 10.3$ mm; $H_{CT} = 7.7$ mm), which may increase precision when deducing the electrode position. Although post-operative MRI scanning is often used routinely to confirm good positioning of the electrodes, concerns regarding the safety of MRI scanning are still often raised [8, 17, 18]. This is because in theory, the presence of a metallic implant carries a potential risk of electrode displacement and of heating under a high magnetic field. The maximal SAR was even lowered by the manufacturer after further experience with the implanted material (SAR ≤ 0.1 W/kg). This kind of issue is obviated when using CT, but safety instructions for radioprotection have to be considered.

CONCLUSION

Post-imaging is becoming more and more important to analyse the final anatomical position of each electrode contact. CT acquisitions run post-operatively in implanted patients provide precise identification of the ends of contact 0 and of contact 3, and given the size of the artefact, result in a precise 3D localisation of the four contacts. These acquisitions offer a useful alternative to MRI, being cheaper and more easily accessible, and they can also be linked to pre-operative anatomical MRI by image fusion.

REFERENCES

1. Benazzouz A, Tai CH, Meissner W, Bioulac B, Bezard E, Gross C (2004) High-frequency stimulation of both zona incerta and subthalamic nucleus induces a similar normalization of basal ganglia metabolic activity in experimental parkinsonism. FASEB J 18:528–530

2. Breit S, Schulz JB, Benabid AL (2004) Deep brain stimulation. Cell Tissue Res 318:275–288

3. Caire F, Derost P, Coste J, Bonny JM, Durif F, Frenoux E, Villeger A, Lemaire JJ (2006) Subthalamic deep brain stimulation for severe idiopathic Parkinson's disease. Location study of the effective contacts. Neurochirurgie 52:15–25

4. Cif L, El Fertit H, Vayssiere N, Hemm S, Hardouin E, Gannau A, Tuffery S, Coubes P (2003) Treatment of dystonic syndromes by chronic electrical stimulation of the internal globus pallidus. J Neurosurg Sci 47:52–55

5. Duffner F, Schiffbauer H, Breit S, Friese S, Freudenstein D (2002) Relevance of image fusion for target point determination in functional neurosurgery. Acta Neurochir (Wien) 144:445–451

6. Erola T, Karinen P, Heikkinen E, Tuominen J, Haapaniemi T, Koivukangas J, Myllyla V (2005) Bilateral subthalamic nucleus stimulation improves health-related quality of life in Parkinsonian patients. Parkinsonism Relat Disord 11:89–94

7. Ferroli P, Franzini A, Marras C, Maccagnano E, D'Incerti L, Broggi G (2004) A simple method to assess accuracy of deep brain stimulation electrode placement: pre-operative stereotactic CT + postoperative MR image fusion. Stereotact Funct Neurosurg 82:14–19

8. Gleason CA, Kaula NF, Hricak H, Schmidt RA, Tanagho EA (1992) The effect of magnetic resonance imagers on implanted neurostimulators. Pacing Clin Electrophysiol 15:81–94

9. Herzog J, Fietzek U, Hamel W, Morsnowski A, Steigerwald F, Schrader B, Weinert D, Pfister G, Muller D, Mehdorn HM, Deuschl G, Volkmann J (2004) Most effective stimulation site in subthalamic deep brain stimulation for Parkinson's disease. Mov Disord 19:1050–1054

10. Krack P, Batir A, Van Blercom N, Chabardes S, Fraix V, Ardouin C, Koudsie A, Limousin PD, Benazzouz A, LeBas JF, Benabid AL, Pollak P (2003) Five-year follow-up of bilateral stimulation of the subthalamic nucleus in advanced Parkinson's disease. N Engl J Med 349:1925–1934

11. Krystkowiak P, Devos D, Dujardin K, Delmaire C, Bardinet E, Delval A, Delliaux M, Cottencin O, Simonin C, Yelnik J, Blond S, Defebre L, Destée A (2007) Impact cognitif et moteur de la stimuation du pallidum externe dans la maladie de Huntington: données préliminaires. Rev Neurol 163:34–35

12. Lemaire JJ, Coste J, Ouchchane L, Hemm S, Derost P, Ulla M, Siadoux S, Gabrillargues J, Durif F, Chazal J (2007) MRI anatomical mapping and direct stereotactic targeting in the subthalamic region: functional and anatomical correspondence in Parkinson's disease. Int J CARS 2:75–85

13. Ondo WG, Bronte-Stewart H (2005) The North American survey of placement and adjustment strategies for deep brain stimulation. Stereotact Funct Neurosurg 83:142–147

14. Pinto S, Le Bas JF, Castana L, Krack P, Pollak P, Benabid AL (2007) Comparison of two techniques to postoperatively localize the electrode contacts used for subthalamic nucleus stimulation. Neurosurgery 60:285–292 discussion 292–294

15. Pollo C, Villemure JG, Vingerhoets F, Ghika J, Maeder P, Meuli R (2004) Magnetic resonance artifact induced by the electrode Activa 3389: an in vitro and in vivo study. Acta Neurochir (Wien) 146:161–164

16. Rezai AR, Phillips M, Baker KB, Sharan AD, Nyenhuis J, Tkach J, Henderson J, Shellock FG (2004) Neurostimulation system used for deep brain stimulation (DBS): MR safety issues and implications of failing to follow safety recommendations. Invest Radiol 39:300–303

17. Schueler BA, Parrish TB, Lin JC, Hammer BE, Pangrle BJ, Ritenour ER, Kucharczyk J, Truwit CL (1999) MRI compatibility and visibility assessment of implantable medical devices. J Magn Reson Imaging 9:596–603

18. Uitti RJ, Tsuboi Y, Pooley RA, Putzke JD, Turk MF, Wszolek ZK, Witte RJ, Wharen RE Jr (2002) Magnetic resonance imaging and deep brain stimulation. Neurosurgery 51:1423–1428 discussion 1428–1431

19. Vayssiere N, van der Gaag N, Cif L, Hemm S, Verdier R, Frerebeau P, Coubes P (2004) Deep brain stimulation for dystonia confirming a somatotopic organization in the globus pallidus internus. J Neurosurg 101:181–188

20. Vercueil L, Pollak P, Fraix V, Caputo E, Moro E, Benazzouz A, Xie J, Koudsie A, Benabid AL (2001) Deep brain stimulation in the treatment of severe dystonia. J Neurol 248:695–700

21. Voges J, Volkmann J, Allert N, Lehrke R, Koulousakis A, Freund HJ, Sturm V (2002) Bilateral high-frequency stimulation in the subthalamic nucleus for the treatment of Parkinson disease: correlation of therapeutic effect with anatomical electrode position. J Neurosurg 96:269–279

22. Wells WM 3rd, Viola P, Atsumi H, Nakajima S, Kikinis R (1996) Multi-modal volume registration by maximization of mutual information. Med Image Anal 1:35–51